Structural Influence of Erbium Centers on Silicon Nanocrystal Phase Transitions

Robert A. Senter,[1] Cristian Pantea,[2] Yuejian Wang,[2] Haozhe Liu,[3] T. Waldek Zerda,[2] and Jeffery L. Coffer[1]

[1]*Department of Chemistry, Texas Christian University, Fort Worth, Texas 76129, USA*
[2]*Department of Physics, Texas Christian University, Fort Worth, Texas 76129, USA*
[3]*HPCAT, Argonne National Laboratory, Argonne, Illinois 60439, USA*

(Received 12 August 2003; revised manuscript received 28 June 2004; published 18 October 2004)

Two different types of erbium-doped silicon nanocrystals, along with undoped, oxide-capped Si dots, are employed to probe the impact of the impurity center location on phase transition pressure. Using a combination of high pressure optical absorption, micro-Raman, and x-ray diffraction measurements in a diamond anvil cell, it is demonstrated that the magnitude of this phase transition elevation is strongly dictated by the average spatial location of impurity centers introduced into the nanocrystal along with the interfacial quality of the surrounding oxide.

DOI: 10.1103/PhysRevLett.93.175502 PACS numbers: 62.50.+p, 61.72.Tt

Often scrutinized for their useful size-dependent optical properties, semiconductor nanocrystals also exhibit intriguing structural phenomena, including melting point depression [1] and phase transition pressure elevation behavior [2,3]. Such characteristics arise from the necessity of finite systems to minimize surface energetics during the transformation event [4]. Silicon (Si) nanocrystals are a particularly important case of such materials, as it has been established that a shape change accompanies the first order phase transition, along with disruption of the $Si - SiO_2$ interface [3]. In this Letter, we demonstrate that the magnitude of this phase transition elevation is dictated by the average spatial location of impurity centers introduced into the nanocrystal along with the interfacial quality of the surrounding oxide.

One particular type of Si nanophase material of current interest involves a crystalline Si host containing erbium impurity centers. Erbium is of interest because of the $(^4I^{13/2}) \rightarrow (^4I^{15/2})$ ligand field transition and the resulting luminescence band at 1.54 μm which lies at an absorption minimum for silica based optical fibers and glasses [5,6]. A Si-based nanoscale light emitter whose luminescence originates from Si exciton-mediated energy transfer with rare earth centers such as Er^{3+} could prove useful for the construction of a monolithic Si-based optoelectronic device. In our laboratory, two different types of doped Si nanocrystals have been synthesized: one involving a random distribution of erbium centers throughout the nanocrystal [7]; the other forces erbium into a location preferentially enriched near the surface [8]. The fact that we can produce Si nanocrystals containing erbium in two distinctively different structural environments provides a useful comparison as to the role of a rare earth impurity center on the phase behavior of this technologically crucial material.

Bulk crystalline Si has a diamond cubic crystal structure at atmospheric pressure and ambient temperatures, and transforms from cubic to the β-tin structure at approximately 12 GPa [9–12]. At 13 GPa this phase is converted to a body-centered orthorhombic structure termed Imma [13,14], followed by a transformation at 16 GPa whereby the Si adopts a primitive hexagonal structure [15,16]. Convenient experimental probes of the first order phase transition exist, including optical absorption in the visible region of the spectrum. As the semiconducting cubic phase of crystalline Si is transformed to the metallic β-Sn (or primitive hexagonal in the case of nanocrystals), a loss of transparency occurs with a corresponding increase in the optical density of the sample [17]. Raman spectroscopy serves as a complementary probe to this type of measurement, as the diminution in intensity of the 520 cm^{-1} phonon for the cubic phase of Si can be monitored [18]. Hence these experiments also address an unanswered question as to the impact of the Er^{3+} centers on the structural integrity of the Si nanocrystal.

Nanocrystals of both randomly dispersed erbium-doped Si and Si nanocrystals with erbium-rich surfaces were prepared by the controlled pyrolysis of diluted Si_2H_6 in He along with vapor of the compound $Er(thmd)_3$ at 1000 °C, achieving erbium incorporation levels of approximately 2 at.% [7,8]. As a control, undoped Si nanocrystals were prepared by employing identical reaction conditions during synthesis, except for the deliberate absence of the erbium source compound. These Si-containing nanocrystals were structurally characterized by a combination of transmission electron microscopy [7,8,19], selected area electron diffraction, energy dispersive x-ray analysis [7,8,19], and extended x-ray absorption fine structure methods (EXAFS) [8,20]. The average diameter of the undoped Si nanocrystals was 18 nm, the randomly dispersed Er-doped Si NCs was 6 nm, and that of the erbium surface-enriched product was ~26 nm; particle size dispersity is on the order of 25%. Pressure is applied to these samples with the use of a diamond anvil cell of Merrill-Bassett design (for Raman) or compact cylinder (for optical absorption), with ethylene glycol or methanol/ethanol/water used as a pressure-

transmitting medium. Pressure calibration was achieved using measurements of the R_1 and R_2 fluorescence lines of ruby [21]. All diamond anvil cell experiments were performed under dilution conditions where shear-induced effects brought about by particle agglomerates are assumed to be negligible.

Fig. 1 illustrates the effect of high pressure, up to 20 GPa, on a set of typical absorption spectra for silicon nanocrystals (of average diameter 26 nm) that possess an erbium-rich surface layer. At the outset, the sample appears light brown with the featureless absorption tail of an indirect gap semiconductor. While there is an initial sluggish increase in optical density (below 5 GPa), with increasing pressure the sample does begin to visibly darken. By 19 GPa it is evident that the dielectric response of this Si nanocrystal sample has been dramatically altered, now reflecting light in the visible or near IR region. Using a working definition of the transformation pressure as the midpoint of integrated optical density values yields a value of 14.9 GPa for this type of sample. While reversible, significant hysteresis is also evident, both in an examination of the raw data (see upstroke spectrum at 14.7 GPa and downstroke spectrum at 5.8 GPa) as well as the integrated optical density (OD) plot [Fig. 1(b)].

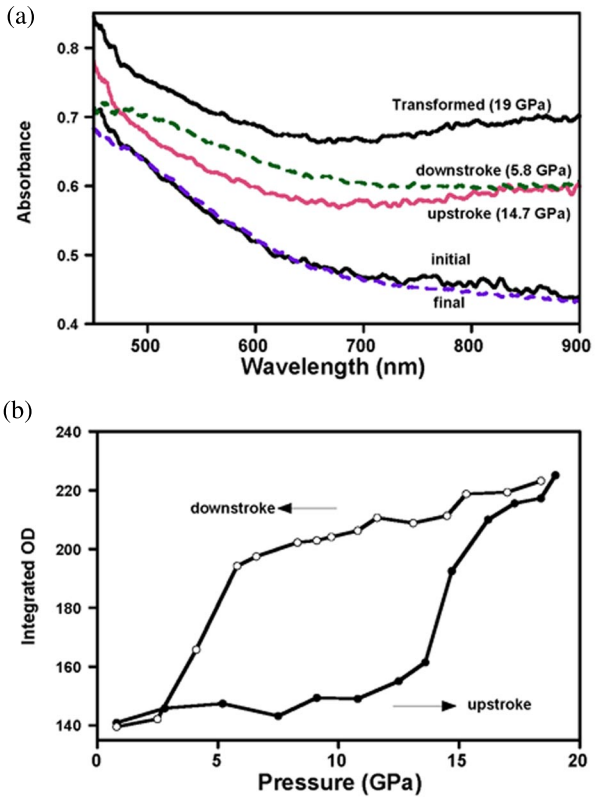

FIG. 1 (color online). (a) Absorption spectra for Er^{3+} surface-enriched Si nanocrystals as a function of increasing and decreasing pressure; (b) Integrated optical density data for the same experiment.

Such measurements are complemented by an evaluation of the pressure-induced diminution of the phonon mode associated with the cubic phase of Si, appearing near 520 cm^{-1} at atmospheric pressure. Raman spectroscopy confirms that the changes in optical density are due to a loss in diamond cubic symmetry of the Si nanocrystals as the pressure is increased. Figure 2 illustrates selected Raman spectra over a typical pressure range for the 18 nm nanocrystallites; a dramatic drop in intensity is easily seen and correlates well with the change in OD shown above.

While known from the literature that the Raman bands associated with Imma and β tin phases of Si are quite weak in intensity but nevertheless fundamentally active [22], it should be pointed out that only an amorphous phase was detected upon the release of pressure; such observations are consistent with previous measurements detecting only this phase upon release for undoped, oxide-capped Si nanocrystals [3] and explains the rather substantial hysteretic character detected in Fig. 1.

Figure 3 compares the upstroke pressure behavior (with regard to changes in OD) of undoped Si nanocrystals, Si nanocrystals with Er^{3+} enriched at the surface, and Si

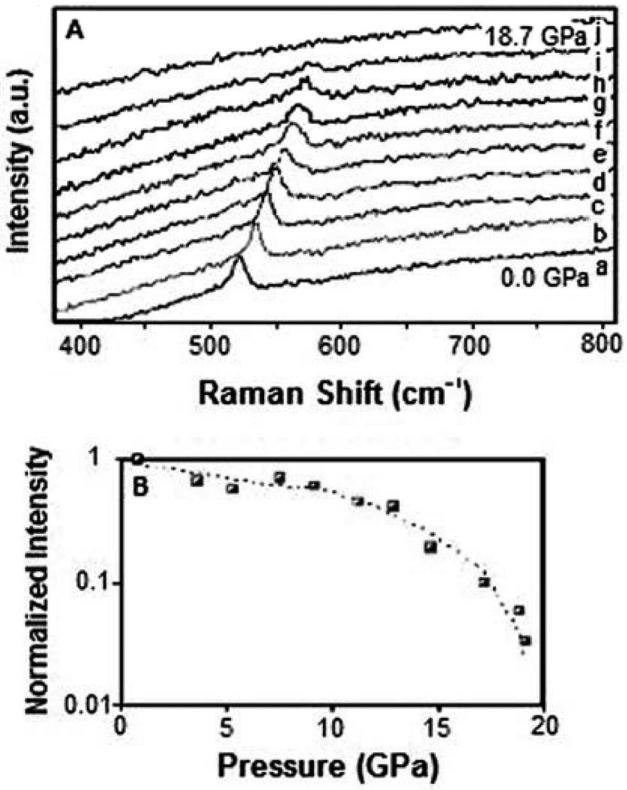

FIG. 2. (a) Typical Raman spectra for 18 nm undoped Silicon nanocrystals at pressures a: 0.0 GPa, b: 3.6 GPa, c: 5.2 GPa, d: 7.5 GPa, e: 9.1 GPa, f:11.1 GPa, g: 12.0 GPa, h: 4.5 GPa, i: 17.0 GPa, j: 18.7 Pa; (b) Logarithmic plot of Raman intensity versus pressure for this type of sample.

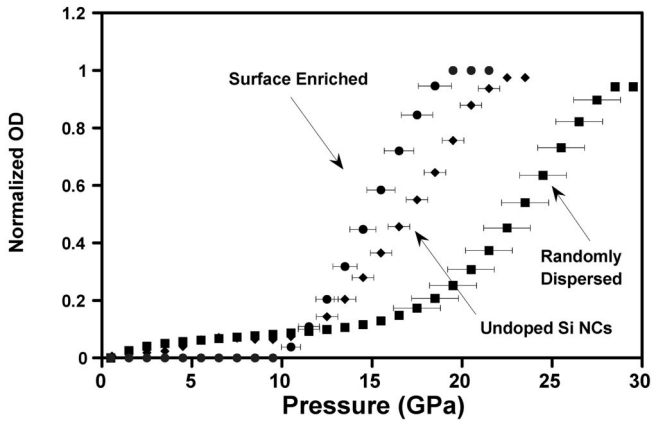

FIG. 3. A comparative plot of integrated OD as function of pressure for (a) Er^{3+} surface-enriched Si nanocrystals (inverted triangles); (b) undoped Si nanocrystals (squares), and (c) randomly dispersed Er^{3+}-doped Si nanocrystals (circles).

nanocrystals with erbium randomly dispersed throughout. While all share the common element of being elevated relative to bulk Si (at 11 GPa), it is also clear that the magnitude of each value depends strongly on sample composition.

We begin with an analysis of ca. 18 nm oxide-capped Si nanocrystals that lack any erbium dopant centers. From the integrated OD plot it is clear that the first order transformation pressure at 16.9 GPa of these nanocrystals is lower than the 21 GPa value originally reported by Alivisatos and coworkers [3]. Recognizing that elevated phase transitions in nanocrystalline systems are transition path-driven phenomena strongly influenced by the energy barrier to reorganization of lattice planes at curved surfaces [4], we surmised that the quality of the as-prepared $Si-SiO_2$ nanocrystal interface could account for the difference between the two systems. In the studies reported earlier, the Si nanocrystals were oxidized in an acidic aqueous solution containing H_2O_2 at 110 °C in order to produce a passivated surface oxide [3]. It should be emphasized that in previous reports there was no apparent size dependence differences in transition pressure for nanocrystals ranging from ten to 50 nm, possibly due in part to strong overlap in size distributions for Si nanocrystals that in general impact size insensitivity. After evaluating some simple plasma and solution oxidation routes, we choose a relatively higher temperature (400 °C) anneal at low vacuum (10^{-3} torr) for passivation of the nanocrystals. While leaving the core nanocrystal size unchanged, the effect of such ananneal is quite striking, shifting the transition pressure from 16.9 to 19.8 GPa (not shown).

For the case of the Si nanocrystals containing Er^{3+} centers (2%) randomly dispersed throughout the cubic structure, it is evident from Fig. 3 that this type of sample has the largest elevation of transition pressure, ~ 23 GPa (relative to both bulk Si as well as the other forms of nanocrystalline Si). At face value this suggests that the presence of such impurity centers in the nanocrystal stabilizes the transition state pathway required for lattice reorganization, thereby shifting it to an even higher pressure. Given the magnitude of this elevation, it is reasonable to raise the possibility that the transformation pathway has been altered from the expected cubic to hexagonal (for a nanocrystal) to cubic to another phase (Imma etc.). Hence we examined the phase transition behavior of these nanocrystals via high pressure x-ray diffraction at the Advanced Photon Source. It is evident that upon reaching values at or above the transformation pressure, the diffraction peaks associated with the primitive hexagonal phase have clearly appeared at 10.31°, 10.75°, and 14.8369° (Fig. 4). Since motions of interior atoms dictate the new surface structure in the high pressure phase that is generated during the shape change, then the presence of Er^{3+} centers at interior sites within the lattice clearly affect the energy landscape of the pathway. Previous EXAFS measurements have determined that the identity of such structural anchors (in terms of local coordination in this type of nanocrystal) entail an Er-O-Si linkage, constrained by the interior of the Si cubic host lattice (as evidenced by a lower Er coordination number in smaller nanocrystals) [20]. Such Er-O complexes are known to fit structurally at interstitial sites within the Si lattice [23]. In addition to these interior impurity centers, the remaining question of how much this effect is influenced by interfacial defects was addressed in an annealing step carried out under conditions identical to those noted above for the undoped Si NCs. Interestingly, there is no change in the phase transition pressure of these erbium-doped Si nanocrystals, thereby adding additional credence to the hypothesis that the erbium centers are not segregated at the surface but rather sprinkled throughout the nanocrystal and it is this type of

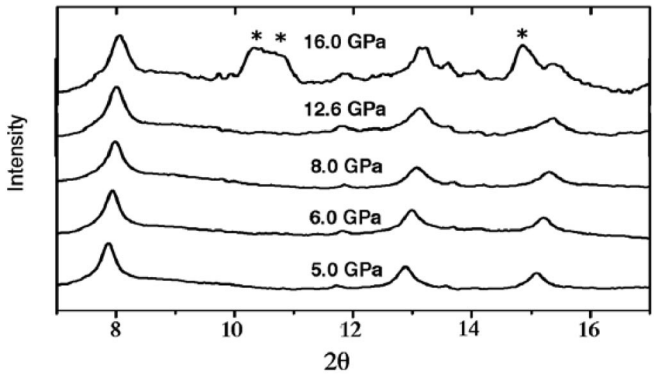

FIG. 4. A series of diffraction data for a randomly dispersed Er-doped Si nanocrystal sample as a function of pressure for the values shown. Diffraction peaks associated with the primitive hexagonal phase at 10.31°, 10.75°, and 14.8369° are marked with asterisks.

Er-O structure that dominates the anchoring effect of the elevation of the phase transition pressure. Next we examine the behavior of Si nanocrystalites that possess a deliberate layer of Er^{3+} ions at the surface (along with oxygen). These 26 nm diameter dots transform at a pressure of 14.9 GPa, still elevated relative to the bulk but clearly suppressed when compared to any of the undoped Si nanocrystal samples noted above. This effect is a combination of two different competing effects: an intrinsic size-dependent elevation arising from the exposed atoms produced via the creation of high index surfaces during a shape change, along with the introduction of new surface defects (associated with Er clustering) that destabilize the Si/SiO_2 interface and subsequently reduce the barrier.

However, the effect of a 400 °C thermal anneal on this type of structure is profound, consistently elevating the magnitude of the phase transition to 23 GPa. Hence there is not only a diminution of Si/SiO_2 defects as a consequence of heating, but it appears that there is a favorable structural attribute which arises when Er^{3+} ions are present in the shell as well.

The radically different phase transition behavior of the as-prepared Er surface-enriched Si nanocrystals, when compared to randomly dispersed Er-doped Si, is consistent with the different Er^{3+} structural environments of these materials. While structure of the erbium centers is oxygen rich for both, previous EXAFS measurements have established a larger coordination number (6.6) for the Er surface rich nanocrystal and longer Er-O atomic separation (2.30 Å) relative to the randomly dispersed Er-doped Si nanocrystals (6.4, 2.30 Å), reflecting a less constrained erbium environment overall (as virtually all of the rare earth centers are located in the first atomic layers of the nanoparticle surface). The effect of the 400 °C anneal on this material however, serves two purposes. While eliminating interfacial defects, the presence of the Er^{3+} near the interface during the anneal adds a subtle level of structural integrity to the shell that slightly elevates the phase transition pressure beyond that of the undoped Si nanocrystals. One can assume that the effect is not coulombic, as any charge imbalance would be present in the as-formed surface layer as well as in the annealed materials. This begs the question of structure-induced effects. It is known from the literature that crystalline erbium silicates of the composition $Er_2Si_2O_7$ possess a linear Si-O-Si bond angle (180°) rather than the well-known tetrahedral silica framework [24]. It is possible that annealing of this Er-containing silicon oxide shell does induce some structural "stiffening" of the Si nanocrystal oxide shell, resulting in a mechanical effect whereby additional force must be applied to deform the shell as well as the reorganize the lattice of the nanocrystal core.

These results are of long-term fundamental significance because they demonstrate that as size diminishes in a finite system, impurity centers and interfacial defects play roles of increasing significance in fundamental structural properties such as phase transitions.

We thank the NSF and Robert A. Welch Foundation for financial support. Use of the Advanced Photon Source was supported by the U.S. Department of Energy under Contract No. W-31-109-Eng-38 and the HPCAT facility supported by DOE-BES, DOE-NNSA, NSF, and DOD-TACOM.

[1] A. N. Goldstein, C. M. Escher, and A. Alivisatos, Science, **256**, 1425 (1992).
[2] C.-C. Chen, A. B. Herhold, C. S. Johnson, and A. P. Alivisatos, Science, **276**, 398 (1997).
[3] S. H. Tolbert, A. B. Herhold, L. E. Brus, and A. P. Alivisatos, Phys. Rev. Lett., **76**, 4384 (1996).
[4] S. H. Tolbert and A. P. Alivisatos, Annu. Rev. Phys. Chem., **46**, 595 (1995).
[5] A. Polman, J. Appl. Phys. **82**, 1 (1997).
[6] J. Michel, L. V. C. Assali, M. T. Morse, and L. C. Kimerling, Semicond. Semimet. **49**, 111 (1998).
[7] J. V. St. John, J. L. Coffer, Y. Chen, and R. F. Pinizzotto, J. Am. Chem. Soc. **121**, 1888 (1999).
[8] R. A. Senter, Y. Chen, J. L. Coffer, and L. R. Tessler, Nano Lett. **1**, 383 (2001).
[9] S. Minomura, H. G. Drickamer, J. Phys. Chem. Solids **23**, 451 (1963).
[10] J. C. Jamieson, Science **139**, 762 (1963).
[11] R. H. Wentorf and J. S. Kasper, Science **139**, 338 (1963).
[12] F. P. Bundy, J. Chem. Phys. **41**, 3809 (1964).
[13] M. I. McMahon, R. J. Nelmes, N. G. Wright, and D. R. Allan, Phys. Rev. B **50**, 739 (1994).
[14] G. A. Voronin, C. Pantea, T. W. Zerda, L. Wang, and Y. Zhao, Phys. Rev. B **68**, 020102(R) (2003).
[15] H. Olijnyk, S. K. Sikka, and W. B. Holzapfel, Phys. Lett. **103A**, 137 (1984).
[16] M. I. McMahon and R. J. Nelmes, Phys. Rev. B **47**, 8337 (1993).
[17] B. Welber, C. K. Kim, M. Cardona, and S. Rodriguez, Solid State Commun. **17**, 1021 (1975).
[18] B. A. Weinstein and G. J. Piermarini, Phys. Rev. B **12**, 1172 (1975).
[19] J. V. St. John, J. L. Coffer, Y. Chen, R. F. Pinizzotto, Appl. Phys. Lett. **77**, 1635 (2000).
[20] L. R. Tessler, J. L. Coffer, J. Ji, and R. A. Senter, J. Non-Cryst. Solids **299-302P1**, 673 (2002).
[21] J. D. Barnett, S. Block, G. J. Piermarini, Rev. Sci. Instrum. **44**, 1 (1973).
[22] V. Dominich and Y. Gogotsi, Rev. Adv. Mater. Sci. **3**, 1 (2002).
[23] A. G. Raffa and P. Ballone, Phys. Rev. B **65**, 121309 (2002).
[24] J. H. Denning *et al.*, Spectrochim. Acta, Part A **28**, 1787 (1972).